Applied Catalysis B: Environmental 197 (2016) 62–72

Contents lists available at ScienceDirect

Applied Catalysis B: Environmental

journal homepage: www.elsevier.com/locate/apcatb

WGS and CO-PrOx reactions using gold promoted copper-ceria catalysts: "Bulk CuO—CeO_2 *vs.* CuO—CeO_2/Al_2O_3 with low mixed oxide content"

T.R. Reina*, S. Ivanova**, O.H. Laguna, M.A. Centeno, J.A. Odriozola

Departamento de Química Inorgánica, Universidad de Sevilla e Instituto de Ciencias de Materiales de Sevilla Centro mixto US-CSIC Avda, Américo Vespucio 49, 41092 Seville, Spain

ARTICLE INFO

Article history:
Received 27 November 2015
Received in revised form 8 March 2016
Accepted 9 March 2016
Available online 10 March 2016

Keywords:
CO-PrOx
WGS
Gold catalysts
Copper-ceria
Bulk *vs.* supported

ABSTRACT

A copper-ceria bulk catalyst has been compared to a series of catalysts designed according to the as called "supported approach", corresponding to the dispersion of low content mixed copper-ceria oxide on alumina matrix. The principal characteristics of both types of catalysts are contemplated and the differences in their electronic and redox properties discussed in details. As a plus, the gold metal promotion of the catalysts is also envisaged. The advantages of the systems in the CO clean up reactions, WGS and CO-PrOx are commented. While the WGS activity appears to be ruled especially by the Cu/Ce surface to volume ratio, the CO-PrOx reaction is governed by the CuO loading. Gold addition provides benefits only at the low temperature WGS regime. Very importantly, the supported systems are always superior to the bulk configuration in terms of specific activity, a key factor from the catalyst's design perspective.

1. Introduction

Following the spirit of this special issue a good example of ceria success and reliability is the CuO—CeO_2 mixed oxide catalyst and its application for CO-clean up goals in the context of hydrogen fuel cells. The overall selectivity in generating a low CO content hydrogen stream required by the PEM fuel cell catalyst is dependent on the efficiency of the catalysts in each segment of the fuel processor [1]. In this sense highly effective catalysts are required for both the water gas shift (WGS) reaction and the preferential CO oxidation (CO-PrOx), which are considered as purification processes for the production of clean hydrogen. This is carried out in fuel processors where WGS and CO-PrOx reactions are coupled as integrated stages. Even several units for every process may be included depending on the design of the fuel processor, in order to maximize the production and the energetic efficiency [2–7]. Herein, CuO—CeO_2 systems have demonstrated outstanding activity for the mentioned reactions and therefore they are intimately linked to the development of the last generation of hydrogen alimented fuel cells [8–13].

To a certain extension the WGS and the CO-PrOx process can be considered as "sister reactions" especially when they are applied to purify hydrogen streams. Even historically, $CuOCeO_2$-like catalysts started to be applied in both reactions almost at the same time. More precisely, the group of Flytzani-Stephanopoulos presented the first report on Cu–CeO_2 for WGS in 2000 [14] while one of the first reports of $CuOCeO_2$ for the CO-PrOx appears in 2001 from Ioannides' group [15].

One of the main advantages of the Cu–CeO_2 for the WGS reaction is its ability to be used as prepared without any previous activation, which is one of the major drawbacks of the traditional $Cu/ZnO/Al_2O_3$ catalysts used in industrial applications [16–18]. The success of $CuOCeO_2$ mixtures for the WGS reaction is also reflected by the high activity exhibited by the inverse CeO_2/CuO catalysts [19]. The excellent catalytic performance of both types of configurations underlines the importance of the metal/oxide interface as a very reactive site where most of the relevant reaction steps take place [20]. Moreover Cu itself is an active metal for the shift reaction and combined with the high oxygen mobility provided by ceria results in an optimum catalyst for the WGS.

Concerning the CO-PrOx reaction, the performance of $CuOCeO_2$ has been compared to that of platinum and gold based catalysts [21]. It was found that nanostructured $CuOCeO_2$ catalyst is superior to noble metal based systems in the low-temperature range, because it has the best compromise between activity, selectivity and price. Furthermore $CuOCeO_2$ based catalysts have demonstrated to be particularly convenient for deposition on diverse

* Corresponding author. Present address: Department of Chemical and Process Engineering, University of Surrey Guildford, GU2 7XH, United Kingdom.
** Corresponding author.
E-mail addresses: t.ramirezreina@surrey.ac.uk, tomas.ramirez@icmse.csic.es (T.R. Reina), svetlana@icmse.csic.es (S. Ivanova).

http://dx.doi.org/10.1016/j.apcatb.2016.03.022
0926-3373/

geometries of structured systems as for example, honeycomb monoliths or microchannel reactors [22,23]. This scalability from powder solids to structured catalysts provides a series of benefits including improved mass and heat transfer and reduced reactor volumes, a critical factor for mobile applications [23].

On the other hand the activity of the ceria based catalysts in both WGS and CO-PrOx can be greatly promoted by the inclusion of small amounts of gold in the catalysts' composition [24–26]. The combination of the high CO oxidation activity of gold nanoparticles and the presence of oxygen vacancies in ceria results in a perfect synergy. For instance, CO can easily interact with Au while H_2O (in the case of WGS) or O_2 (in the case of CO-PrOx) can be activated in the oxygen vacancies of ceria which play a vital role in both reactions. Furthermore, these structural defects are view as preferential sites for gold nucleation facilitating the noble metal dispersion and enhancing the overall activity [24,25]. Apart from the well-studied Au/CeO_2 systems, a multicomponent Au, CuO and CeO_2 catalyst represents an interesting approach [25]. In fact, as recently reported Au–Cu alloys supported on ceria are rather efficient catalysts for the PrOx process [26].

Despite the cited benefits of the inclusion of gold in the formulation of $CuOCeO_2$ catalysts, the addition of a noble metal (even in low quantities) would increase the cost of the final catalyst. However as a way to partially compensate this expense, the amount of copper and ceria can be largely reduced by dispersing the mixed oxide on a high surface carrier. In this sense, recent reports of our group demonstrated that this approach of using alumina as a massive component of the ceria-based catalysts allows optimizing the expense of ceria resulting in highly active catalysts for WGS and PrOx with considerable lower quantities of ceria [27,28]. Greater surface to volume ratio is attained when small ceria particles are dispersed on alumina leading to enhanced oxygen mobility and excellent catalytic skills [28].

For all stated above, in this work we have developed a series of $CuOCeO_2$ catalysts dispersed on alumina with a reduced content of active phase (copper and cerium). These systems have been comparatively studied with a reference $CuOCeO_2$ bulk material for both WGS and CO-PrOx reactions. Moreover, the use of gold nanoparticles as promoter for both processes is also considered. Finally the main reasons guiding the catalytic trends have been discussed and interrelated with the physicochemical properties of the designed materials.

2. Experimental

2.1. Catalyst preparation

2.1.1. $CuOCeO_2$ bulk catalyst

The synthesis of the CuO/CeO_2 bulk catalyst (15 CuO wt.% and 85 CeO_2 wt.%) has been previously published [25] and the co-precipitation method was employed. The required amounts of $Cu(NO_3)_2{\cdot}3H_2O$ (Fluka®) and $Ce(NO_3)_3{\cdot}6H_2O$ (Alfa Aesar®) were dissolved in the adequate amount of distilled water to obtained a 0.5 M solution of the cationic precursors. Later, NaOH solution (2 M) was added dropwise until a stable pH of 9. The obtained precipitate was filtered and washed with distilled water. Then, it was dried overnight at 60 °C and finally calcined at 300 °C (10 °C/min) for 2 h. The sample prepared following this procedure will be labelled as *CuCe bulk*.

2.1.2. $CuOCeO_2/Al_2O_3$ samples

The $CuOCeO_2/Al_2O_3$ samples were synthesized by the co-impregnation method. The necessary amounts of metal nitrate precursors (cerium and copper nitrates, Sigma-Aldrich) were co-impregnated on γ-alumina powder (Sasol). The impregnation was carried out in 50 mL of ethanol, evaporated at reduced pressure in rotary evaporator (Heidolph) at 50 °C till obtaining a dry solid which was subsequently treated with ammonia solution for 10 min. The support dried overnight at 80 °C and calcined at 500 °C during 4 h.

A series of catalysts with remarkable lower $CuOCeO_2$ loading compared to that of the bulk system was prepared using the above described procedure. The catalysts were synthesized using growing CuO/CeO_2 ratios (0.4, 0.6 and 0.8) and a total $CuO + CeO_2$ loading lower than 25 wt.% in all the cases. For sake of simplicity, oxygen is omitted in the selected nomenclature and the samples will be labelled according to their Cu/Ce weight ratio. For example the catalyst labelled as CuCe-0.8 is composed by a mixed $CuOCeO_2$ oxide with a CuO/CeO_2 weight ratio of 0.8 dispersed on alumina.

2.1.3. Gold deposition

Gold was deposited by the direct anionic exchange method (DAE), assisted by NH_3 as described in literature [29]. A 10^{-4} mol L^{-1} aqueous solution of the gold precursor $HAuCl_4$ (Alfa Aesar) was used in order to obtain a final Au loading of 2 wt.%. The support used to prepare the gold based catalysts was sieved and the 100–200 μm fractions retained were employed in the synthesis. After Au deposition, the solid was dried at 100 °C overnight and calcined in air at 350 °C for 4 h.

2.2. Catalyst characterization

X-ray microfluorescence spectrometry (XRMF) was used to determine the chemical compositions and the analysis were performed in EDAX Eagle III spectrophotometer with Rh source of radiation.

X-ray diffraction (XRD) analysis was carried out on X'Pert Pro PANalytical instrument. Diffraction patterns were recorded using Cu Kα radiation (40 mA, 45 kV) over a 2θ-range of 10–80° and using a step size of 0.05° and a step time of 240 s.

The Raman spectra were recorded in a dispersive Horiva Jobin Yvon LabRam HR800 spectrometer, with a 20 mW He–Ne green laser (532.14 nm) operating at 5 mW. The microscope used a 50x objective and a confocal pinhole of 1000 μm.

The UV–vis spectra were recorded on an Avantes spectrometer model AvaLight-DH-S-BAL using $BaSO_4$ as reference. All the spectra were collected in a diffuse reflectance mode and transformed to a magnitude proportional to the extinction coefficient through the Kubelka–Munk function F(α). From UV–vis spectra, ceria direct and indirect band gap were estimated by plotting $[(F(R)h\nu]^{1/2}$ against energy and the linear part of the curve further extrapolated to $[(F(R)h\nu]^{1/2} = 0$ for the indirect gap and the same procedure but using $[(F(R)h\nu]^2$ function was used for the direct band gap.

H_2-TPR was carried out on 50 mg of sample charged in a conventional U-shaped reactor as a function of temperature with constant heating rate of 10 °C min^{-1} till 900 °C. 50 mL min^{-1} certified 5% H_2 in Ar gas mixture was used and the H_2 consumption was followed by TCD detector and quantified by using CuO standard (99,999%).

2.3. Catalytic activity

2.3.1. Water-gas shift

Water-gas shift reaction was performed in a stainless steel tubular flow reactor (0.75 cm ID) at atmospheric pressure in the 180–350 °C temperature range. The catalysts were pelletized and sieved with the 600–800 μm fraction employed for the test. The following conditions were applied: catalyst bed volume 1.5 cm^3, space velocity 4000 h^{-1} and gas composition: 30% vol. H_2O + 4.5% vol. CO balance in N_2. Water was injected into flowing gas stream by HPLC pump, vaporized and homogenized with the gas feed before entering the reactor. This is a model reaction mixture which is usually employed to test catalysts for the clean H_2 production via WGS.

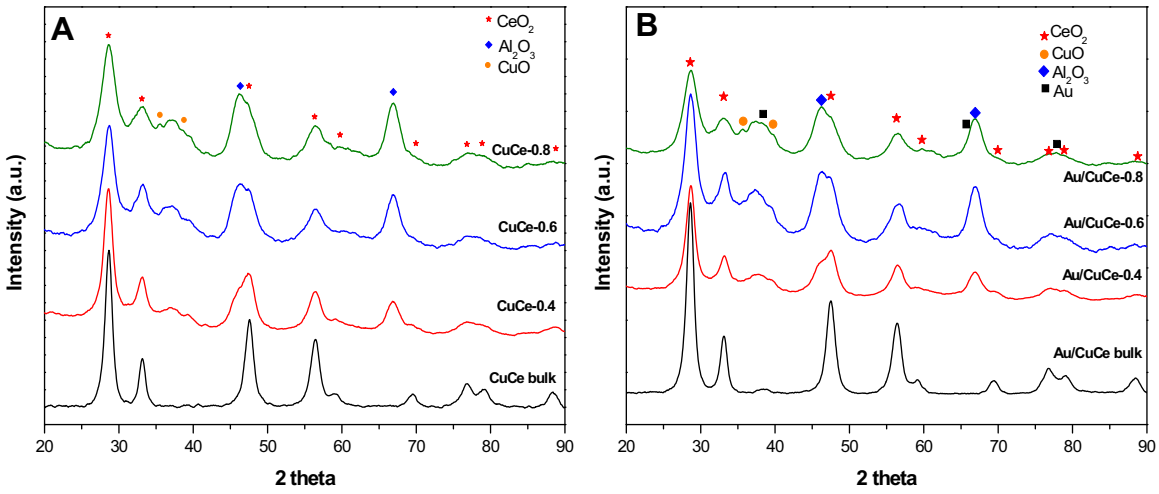

Fig. 1. XRD patterns of the prepared materials. (A) CuCe mixed oxides; (B) gold promoted catalysts.

However, for CO clean-up goals a second reaction mixture using gas composition imitating the outlet of an ethanol reformer: 30% H_2O, 9% CO, 11% CO_2 and 50% H_2 was employed. In all the experiments, CO and CO_2 concentrations were determined by on line ABB gas analyzer and the activity expressed in terms of CO conversion. All the samples were tested as prepared without any previous activation.

2.3.2. CO-PrOx

The preferential CO oxidation reaction was carried out at atmospheric pressure in a stainless steel fixed bed reactor of 9 mm inner diameter, with a 100 mL min^{-1} reaction feed composed by 1% CO, 1% O_2, 50% H_2 and N_2 as balance. The catalysts (100 mg, $100 < \phi < 200$ μm) were diluted with SiC (Prolabo, 125 μm) forming a bed of about 5 mm in length. Products and reactants were separated and quantified by on-line gas chromatography (Agilent® 6890) equipped with HP PLOT Q and HP-5 columns and TCD detector. Prior the catalytic measurements, the samples were treated under a 100 mL min^{-1} flow of air, at 300 °C during 1 h The CO conversion was calculated according Eq. (1) where CO_{in} is the inlet CO concentration and CO_{out} is the outlet one:

$$CO\ conversion\,(\%) = \frac{CO_{in} - CO_{out}}{CO_{in}} \times 100 \quad (1)$$

The selectivity towards CO_2 formation was calculated using Eq. (2) where O_{2in} corresponds to oxygen in the inlet and O_{2out} to outlet concentration.

$$selectivity\,(\%) = \frac{(CO_{in} - CO_{out})}{2x(O_{2in-}O_{2out})} \times 100 \quad (2)$$

In every reaction, the, λ parameter, Eq. (3), was 2:

$$\lambda = \frac{2\,[O_2]}{[CO]} \quad (3)$$

3. Results and discussion

3.1. Chemical composition

The chemical composition of the prepared materials is presented in Table 1. As mentioned above, the intended composition of the samples was defined in terms of the CuO/CeO_2 weight ratio. Nevertheless, during gold deposition the samples are usually treated with ammonia solution, which imposes the condition to our catalysts to be pretreated in ammonia in order to stabilize the Cu/Ce ratio before Au addition. In these conditions leaching of both Cu and Ce is expected to occur, and indeed small discrepancies between the nominal and the actual CuO/CeO_2 ratio were observed. In particular a slight decrease on CuO upon gold deposition is observed. Such a decrease in CuO is more dramatic for the CuCe bulk sample which loses 25% of CuO after gold addition. Considering the highly basic media due to the use of ammonia during the preparation process, some leaching of the loosely attached copper precursors could occur explaining the observed copper depletion.

Table 1
Chemical composition of the prepared catalysts.

Sample	CeO_2 (wt.%)	CuO (wt.%)	Au (wt.%)	CuO/CeO_2 weight ratio
CuCe-0.4	7.7	3.1	–	0.40
Au/CuCe-0.4	8.1	3.3	1.5	0.40
CuCe-0.6	13.9	9.2	–	0.66
Au/CuCe-0.6	13.9	7.7	1.4	0.55
CuCe-0.8	13.8	10.6	–	0.76
Au/CuCe-0.8	13.5	9.4	1.9	0.70
CuCe bulk	84.2	15.8	–	0.18
Au/CuCe bulk	86.5	11.7	1.8	0.14

Regarding gold loading, all the gold promoted catalysts presented a noble metal loading close to the targeted value confirming the successful gold deposition using the direct anionic exchange method.

Although not shown in the paper, other important difference between CuCe bulk and the rest of the samples is the greater specific surface area of the alumina supported materials (around 200 m^2/g) compared to that of the CuCe bulk (close to 80 m^2/g).

3.2. XRD

X-Ray diffraction was used to analyze the crystalline phase composition of the prepared materials. Fig. 1 presents the XRD diffraction patterns of the $CuOCeO_2$ based catalysts (Fig. 1A) and the gold promoted samples (Fig. 1B). For the mixed oxides dispersed on alumina, all the XRD profiles are governed by the typical diffractions of the primary support γ-Al_2O_3 (JCPDS 10-0425) [30] and the common diffraction peaks of ceria fluorite cubic structure (JCPDS 34394) [31]. In addition, although smooth and with low intensity, some peaks related to monoclinic CuO (JCPDS 45-0937) [32] were detected for these samples indicating the presence of CuO on the surface. For the CuCe bulk sample, only diffraction lines corresponding to the FCC—CeO_2 fluorite structure were observed. No peaks belonging to CuO or any other ordered Cu containing phases

Table 2
Miscellaneous features of the studied samples. CeO_2 crystallite size (D) and lattice parameter (a). Estimation of oxygen vacancies population (Ov/F_{2g} ratio) and ceria direct and indirect band gap. Reducibility percentage (RP).

Sample	[a]Crystallite size D (nm)	[b]Cell parameter a (Å)	[c]O_v/F_{2g} area ratio	Direct band gap (eV)	Indirect band gap (eV)	RP (%)
CuCe-0.4	6.7	5.401	0.60	2.88	2.50	71.8
Au/CuCe-0.4	6.5	5.400	0.53	2.67	2.21	53.8
CuCe-0.6	4.9	5.394	0.98	2.97	2.25	55.1
Au/CuCe-0.6	4.8	5.398	0.82	2.56	1.85	60.1
CuCe-0.8	4.5	5.397	1.42	2.83	2.34	44.5
Au/CuCe-0.8	4.6	5.395	1.19	2.28	1.70	46.4
CuCe bulk	8.1	5.396	0.06	2.97	2.52	24.5
Au/CuCe bulk	7.7	5.394	0.04	2.68	2.23	16.1

[a] Calculated from XRD data, with Scherrer's equation and (111) crystallographic plane.
[b] Calculated from XRD data, with Bragg's equation for a cubic cell.
[c] Calculated from Raman Spectra.

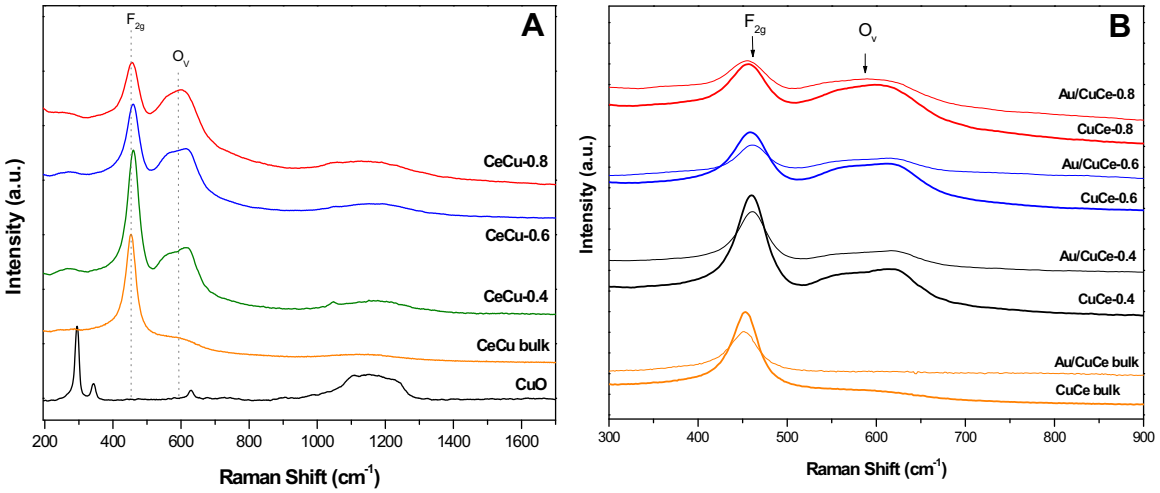

Fig. 2. Raman spectra of the synthesized solids. (A) CuCe mixed oxides; (B) gold promoted catalysts compared with CuCe mixed oxides.

were detected in this sample. This could be a consequence of a high CuO dispersion and also lower scattering factor of CuO compared to CeO_2 when CuKα wavelength is used for the analysis [33].

Moreover, the inclusion of Cu into the ceria lattice forming solid solution could not be completely discarded. It has been broadly reported that the solubility of copper in the ceria lattice heavily depend on the preparation method and calcination conditions [14,34,35]. For further clarification the lattice constants of ceria were estimated and presented in Table 2. It seems very clear that all the samples exhibit a certain degree of ceria lattice contraction, since the a parameter is always inferior than the typical one for a pure cubic ceria (5.4060 Å) [36]. The replacement of Ce^{4+} ion (97 pm, CN = 8) by Cu^{2+} ion (73 pm, CN = 6) should impose a contraction on the cubic cell. Increase of the cell contraction with the decrease of the Cu/Ce ratio is observed, suggesting different Cu/Ce interactions in a way that higher the copper content higher the interaction and higher the degree of Cu dissolution. The latter could explain the observed CuO diffractions in some of the samples. At the same time this substitution phenomenon involves the formation of oxygen vacancies to compensate the charge balance which in turn results in an opposite effect on the lattice parameter (oxygen vacancies tend to expend the ceria cubic cell) [37,38]. In this situation, $CuOCeO_2$ solid solution can be proposed for our systems but the magnitude of Cu inclusion in ceria lattice is difficult to foresee in light of the XRD data due to the above mentioned contradictory effects. In any case the absence of copper diffractions in the CuCe bulk sample and the presence of such peaks in the supported materials indicate a different dispersion and/or copper-ceria interaction in both configurations.

Further interesting information extracted from XRD is the CeO_2 particle size. As shown in Table 2 the samples dispersed on alumina present smaller ceria crystallite size compared to the CuCe bulk catalyst. This result is relevant since smaller ceria particles drive to a greater Cu/CeO_2 interface which is crucial for an enhanced activity in this type of processes [19]. Among the CuCe mixed oxides supported on alumina a clear trend can be established in such a way that higher the Cu atomic loading smaller the ceria particle size. This tendency is in fair agreement with previous results obtained Liu et al. [39] who observed a gradual CeO_2 size decrease upon increasing Cu loading from 2 at.% to 15 at.% and could indicate a stronger Cu–Ce contact for high Cu loadings.

As for the gold promoted catalysts, no diffractions peaks attributed to any gold crystalline species were detected for all studied samples indicating a well dispersion and small noble metal particles size in good agreement with previous results in literature using the ammonia assisted-DAE method for gold deposition [26–28]. Also the addition of gold did not sensitively influence on the ceria crystallite size and the fluorite lattice dimension.

3.3. Raman spectroscopy

Raman spectroscopy of fluorite type oxide structures are dominated by oxygen lattice vibrations, which are sensitive to the crystal symmetry, thus being a potential tool to obtain additional structural information [40]. Indeed, interesting differences between the bulk $CuOCeO_2$ and the supported $CuOCeO_2/Al_2O_3$ samples can be established from the Raman study. Fig. 2A shows the Raman spectra of the prepared CuCe catalysts. All samples exhibit a main band centred at about 462 cm^{-1}, which is assigned to Ce F_{2g} mode due to

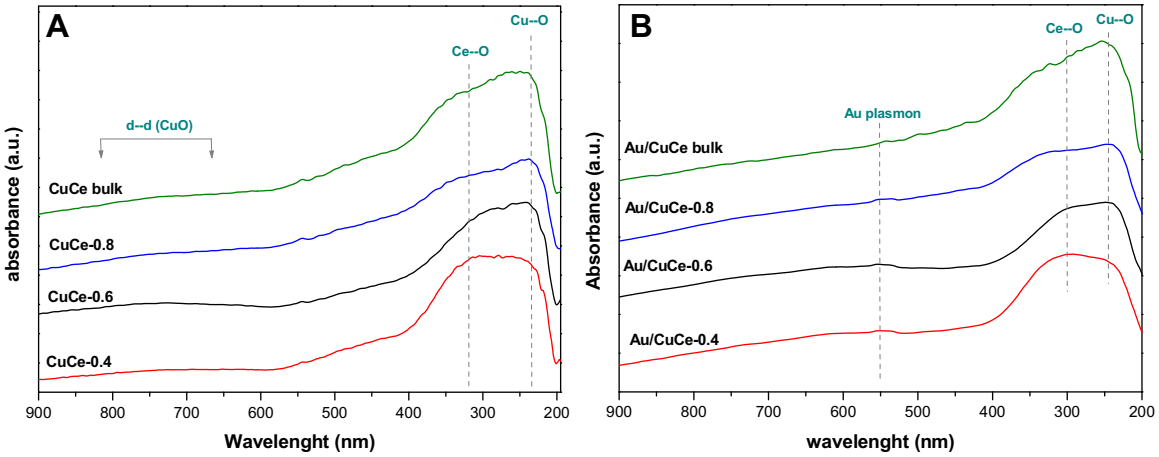

Fig. 3. UV-vis spectra. (A) CuCe mixed oxides; (B) gold promoted catalysts.

symmetrical stretching of Ce–O vibrational unit in octahedral coordination [40,41]. As reported by Graham et al. [42], broadening and shifting of this band indicates variations in ceria particle size. In our case we observed a blue shift of the F_{2g} mode for the CuCe catalysts dispersed on alumina compared to the CuCe bulk sample. Typically blue shift is ascribed to a decrease on the average ceria particle size in good concordance with the XRD data discussed above.

In addition, a weak band ca. 260 cm^{-1} and another pronounced band at approximately 600 cm^{-1} were detected. These phonons have been previously attributed, to the normal Raman inactive (IR active) transverse and longitudinal optical phonon modes at the Brillouin zone centre respectively [43]. The band centred at 600 cm^{-1} is especially relevant to discern the defect chemistry of ceria. Normally, this mode should not be observed by Raman Spectroscopy; however, the presence of some defects can involve relaxation of the selection rules. In particular, this band has been linked to oxygen vacancies (O_v) in the CeO_2 lattice [44], and is considered generally as an evidence for the solid solution formation. Indeed if Cu^{2+} substitutes Ce^{4+} oxygen defects should be created to balance the charges. In other words, Raman spectra could confirm the preliminary conclusions extracted from XRD data about the possible existence of the Cu-Ce solid solution.

Beyond the solid solution detection it is more valuable to compare the intensity and the shape of this band in the studied systems in order to identify more discrepancies among CuCe bulk and alumina based solids. A detailed glance on the band shape reveals the presence of the least two components, the vacancy band described above and a new one blue shifted in respect to the later. The presence of cuprous oxide (Cu_2O) Raman active modes could be responsible for that presenting a vibration centred at 550 cm^{-1} [45,46]. The later seems to be certain in a great extent as the asymmetricity of the band tends to lower Raman shifts. In any case, no matter the band contribution oxygen vacancy or cuprous oxide formation this band evokes the oxide's defect chemistry. As depicted in Fig. 2B the intensity of the O_V band is higher by far when CuCe is dispersed on alumina than when CuCe is prepared as a bulk material. This information could suggest either greater concentration of oxygen vacancies for the alumina based materials compared to the CuCe bulk, or the presence of some Cu_2O. It should be mentioned also that this band is also influenced by the ceria particle size and generally its intensity grows up when ceria size decreases [47] which correlates fairly well with our Scherrer calculations. The calculation of the ratio of the oxygen vacancies band and the F_{2g} signal areas (O_v/F_{2g}) is well-accepted approach to evaluate ceria oxygen vacancies concentration [48,49]. As indicated in Table 2 all the copper-ceria samples supported on alumina exhibit larger concentration of oxygen vacancies than the copper-ceria bulk system with a O_v/F_{2g} ratio more than one order of magnitude bigger. This is a remarkable difference between both types of configurations. Despite their low mixed oxide content, highly defective ceria based solids are obtained when $CuOCeO_2$ mixtures are dispersed on a high surface carrier as alumina, an advantageous feature given the role played by these punctual defects in oxidation reactions. Moreover it is important to note that among the alumina supported catalysts the O_v/F_{2g} is influenced by the Cu/Ce ratio in such a way that higher the Cu/Ce proportion, bigger the O_v/F_{2g} factor. Hence it can be partially concluded that Cu richer mixtures present a higher amount of oxygen vacancies.

Nevertheless the Raman spectra in Fig. 2B also reveal the presence of some CuO active modes, in particular for Cu/Ce ratio of 0.4. Cupric oxide belongs to the C^6_{2h} space group with two molecules per primitive cell and presents 3 main active Raman modes Ag +2Bg. As previously reported, the band at 288 cm^{-1} to the Ag mode and the peaks at 336, 620 cm^{-1} to the Bg modes [50]. All of these bands are either weak or overlapped with ceria Raman modes. Additionally, a broad band centred at 1150 cm^{-1}, assigned to multi-phonon (MP) transition was observed for the alumina based systems [51]. The presence of the CuO Raman mode is in agreement with our XRD data, where some CuO phases were detected. Although the presence of CuO could contribute to the Ce oxygen vacancy band it should be mentioned that within the supported systems, higher the Cu/Ce ratio lower the CuO contribution and higher the vacancy band and Cu_2O contributions.

The addition of gold, cause an impact in the Raman profiles in particular altering the intensity of the main ceria bands (F_{2g} and O_v) as indicated in Fig. 2B. Indeed the calculation of the O_v/F_{2g} points a systematic diminution of this parameter upon gold deposition. Such a phenomenon have been previously observed and attributed to the preferential nucleation of gold particles on the oxygen vacancies of ceria [52]. Somehow this Au–O_v interaction correlates well with the observed gold uptake in Table 1 which reveals that the sample with the higher oxygen vacancies population (CuCe-0.8) is the one with the maximum gold loading.

3.4. UV–vis

Further insights on the electronic properties of the prepared systems were obtained by UV–vis spectroscopy. Fig. 3 presents the UV–vis spectra of the studied materials. For the $CuOCeO_2$ mixed oxides all the samples present a rather similar profile with 3 main common bands (Fig. 3A). For example all the solids shows a broad band at around 300 nm ascribed to the charge transfer from 2p

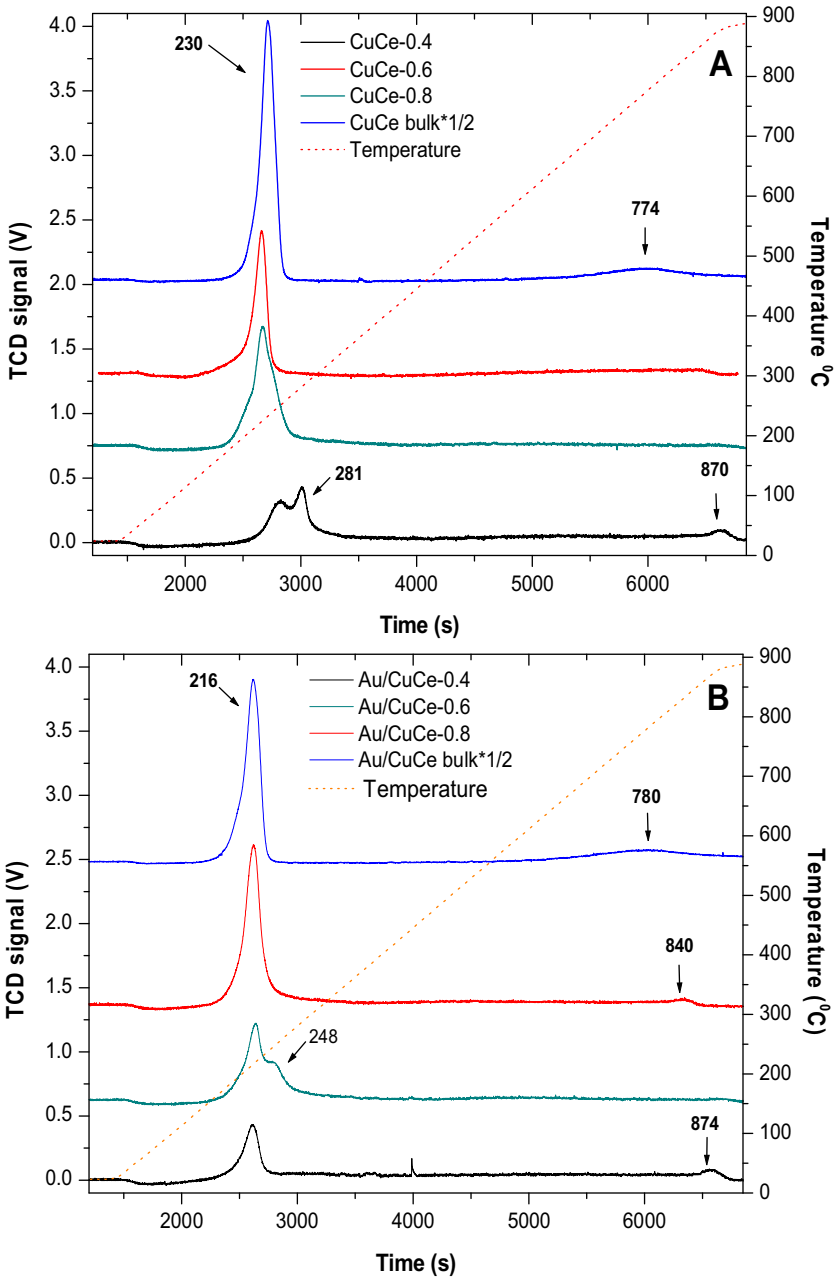

Fig. 4. H_2-TPR profiles. (A) CuCe mixed oxides; (B) gold promoted catalysts.

valence band of O^{2-} to 4f band of Ce^{4+} [53] This band is slightly shifted and widened depending on the samples composition evidencing different Ce–O environments in good agreement with the demonstrated diversity of oxygen vacancies population.

Along with ceria bands, copper oxide absorptions are present in the spectra. For instance a pronounced band around 250 nm due to the charge transfer band from 2p levels of O^{2-} to 3d orbitals of Cu^{2+} is observed [54]. It should be mentioned that this band could overlap with $O \rightarrow Ce^{3+}$ charge transfer reported at around 250 nm for nanosized defective ceria which is expected according the high concentration of oxygen vacancies detected by Raman [55]. Within the alumina based catalysts this band at 250 nm seems to be more pronounced when the Cu/Ce ratio increases in good agreement with the O_v/F_{2g} values in Table 2 indicating the contribution of defects level of ceria in the UV-spectra. In addition, a broad band ascribed to the copper d–d transitions in the 500–800 nm zone is also intended for the samples [56].

Concerning gold promoted catalysts, the presence of the noble metal did not alter too much the UV–vis spectra of the $CuOCeO_2$ mixed systems (Fig. 3B). The shape of Cu–O and Ce–O absorption edges is slightly modified indicating a gold/copper-ceria interaction. Furthermore a new band is found showing a maximum in the range 550 nm for the studied samples which is assigned to the well-known plasmon resonance of the gold nanoparticles [57].

Perhaps more interesting than the UV–vis absorptions profiles, is to examine the band gap trends on this materials. Indeed, band gap in semiconductors oxide provides an idea of the overall basicity which is fundamental to understand the adsorbate-catalyst interactions. Generally speaking, basicity increases oppositely to band gap energy [58]. As shown in Table 2 the direct band gap of the CuCe mixed materials (both alumina supported and bulk) fluctuates between 2.83 and 2.98 eV which is a bit lower to the typical value for pure ceria (3.10 eV) [59]. The band gap contraction reflects the Cu–Ce intimate contact and it is very likely due to the

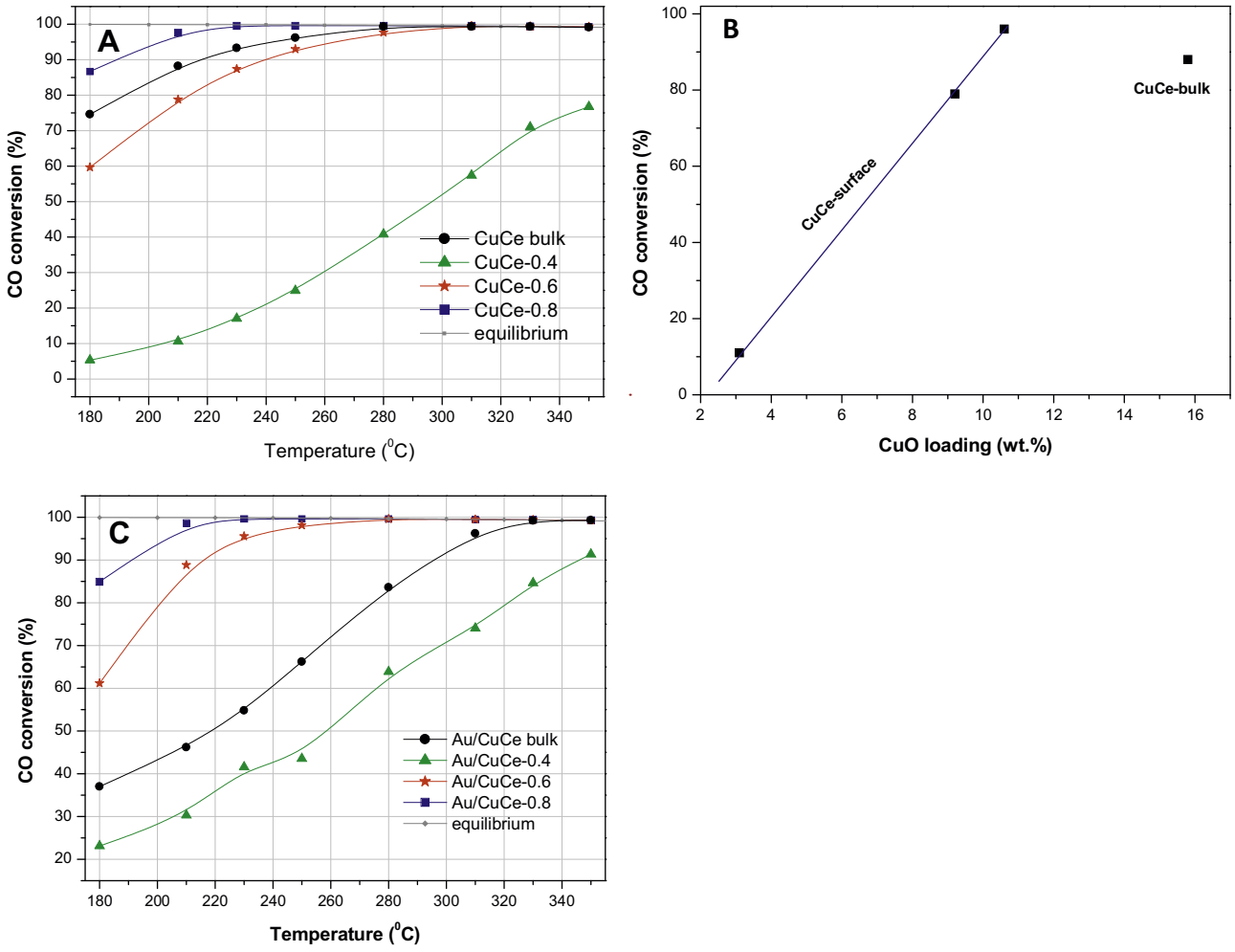

Fig. 5. Catalytic behaviour in the WGS reaction using a model mixture (30% H_2O + 4.5% CO balanced in N_2) (A) CuCe mixed oxides; (B) activity at 210 °C of the prepared mixed oxides; (C) gold promoted catalysts.

Table 3
CO-PrOx and WGS specific reaction rates at 130 °C and 180 °C respectively. All the values are referred to the amount of active phase which is considered the sum in moles of Au, CuO and CeO_2 in the multicomponent catalysts.

Sample	CO-PrOx rates (mol CO converted/s × mol active phase × 10^{-4})	WGS rates (mol CO converted/s × mol active phase × 10^{-4})
CuCe bulk	6.58	2.25
CeCu-0.4	13.80	1.24
CeCu-0.6	10.43	4.69
CeCu-0.8	4.65	6.13
Au/CuCe bulk	7.32	1.31
Au/CeCu-0.4	21.67	4.87
Au/CeCu-0.6	13.02	5.41
Au/CeCu-0.8	4.29	6.57

inclusion of Cu electronic levels in between ceria valence and conduction band. Also the creation of a defects band lying between ceria HOMO-LUMO orbitals as a result of the oxygen vacancies formation is plausible and could contribute to the band gap contraction. Very interestingly, the band gap value remarkably drops upon gold addition evidencing a strong noble metal-support electronic interaction. This electronic metal-support interaction has been proposed as a key parameter to explain catalytic trends [60]. In fact the electronic interchange at the noble metal-support interface may modulate the electronic density of the catalyst's surface tuning the ability of the catalysts to interact with the reactant molecules [61]

3.5. Redox properties: H_2-TPR

Preferential CO oxidation and water gas shift are complex oxidation processes that require catalysts with oxygen mobility and enhanced redox properties. In this sense, H_2-TPR experiments of the studied samples were carried out to evaluate the catalysts' redox properties and the interaction among the active species. Fig. 4A shows the TPR profiles of the Cu–Ce catalysts. Significant discrepancies can be established between the CuCe bulk material and the CuCe samples dispersed on alumina. Regarding the reduction events, all the samples present a marked reduction peak centred

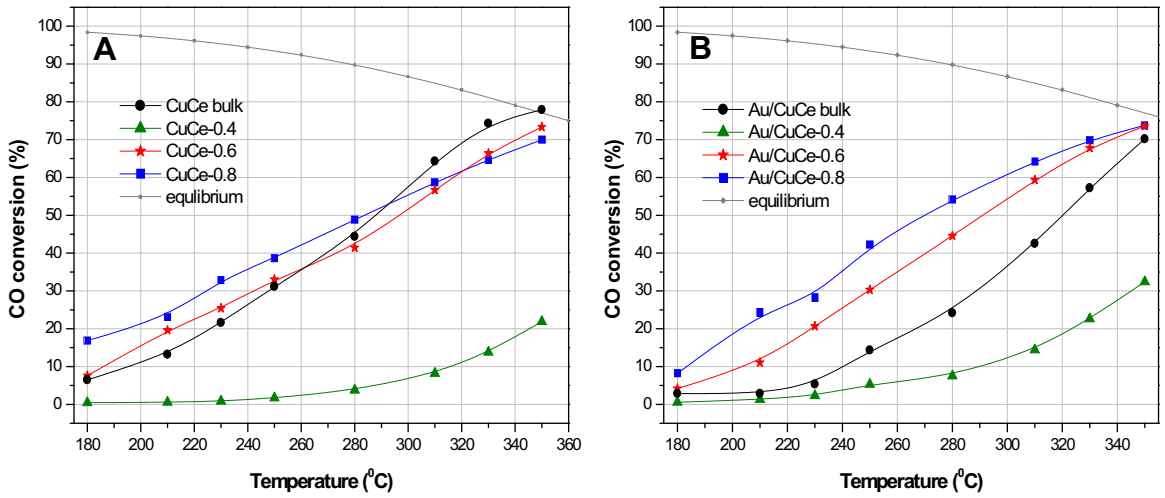

Fig. 6. Catalytic performance in the WGS reaction using a post-reforming mixture (50% H_2; 12% CO_2; 30% H_2O; 11% CO) (A) CuCe mixed oxides; (B) gold promoted catalysts.

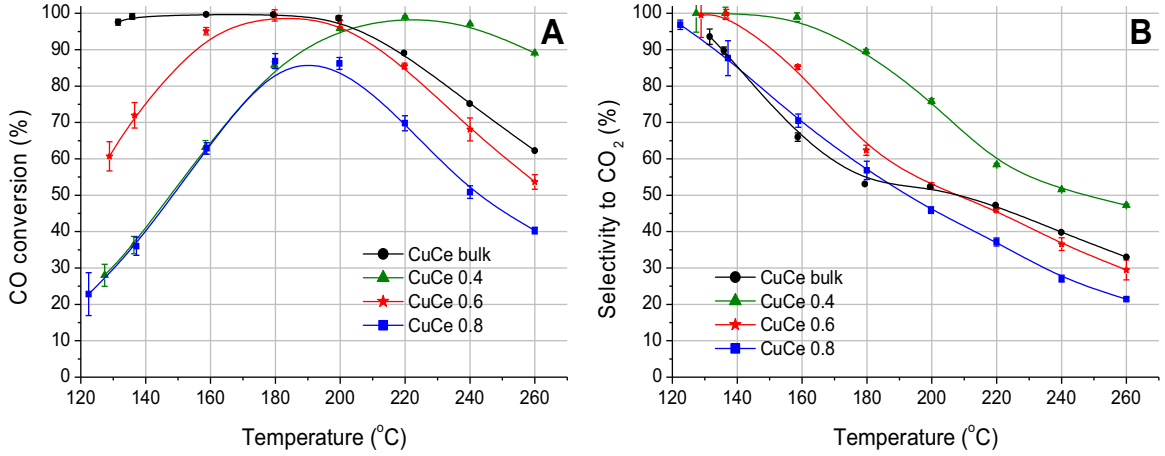

Fig. 7. Catalytic screening in the CO-PrOx reaction of the prepared CuCe materials. (A) CO conversion; (B) selectivity towards CO_2.

at 230 °C which can be assigned to the simultaneous reduction of Cu^{2+} to Cu and the Ce^{4+} surface reduction. Although ceria surface reduction is frequently reported to happen at higher temperatures (*ca.* 400 °C) [62] for $CuOCeO_2$ mixed oxide this reduction takes place at much lower temperatures due to the strong Cu effect on the Ce reduction [33]. Curiously, this reduction process is delayed and split in two components for the CuCe-0.4 sample with a pronounced peak at 281 °C. Probably poorer Cu-Ce synergy is obtained for these samples allowing the separation of the CuO and ceria surface reduction. In the high temperature range a second reduction event appears with a maximum at 774 °C for the CuCe bulk sample which is related to bulk ceria reduction [62]. This process was not detected for the mixed oxides supported on alumina except in the case of CuCe-0.4. Apparently, CuCe-0.6 and CuCe-0.8 only present ceria surface reducibility (merged with copper reduction) which actually is the most relevant for the targeted reactions.

The addition of gold (Fig. 4B) did not modify significantly the high temperature reduction zone and the profiles in this part of the plot resemble those of the samples without noble metal. However the low temperature reduction processes are shifted towards lower temperatures in all the cases. In fact, the presence of gold is often reported to facilitate the H_2 mobility and also to weaken the Ce-O bond due to the electronic transfer between the oxide and the noble metal resulting in an overall improved reducibility [63,64]. Moreover, as stated by Jacobs et al. [65] the enhanced support reduction in noble metal-ceria systems not only involves the shifting of the reduction processes to lower temperature, but also the extent of reduction. The surface reduction is critical for generating the active geminal OH groups on the surface of the ceria which plays a fundamental role in the WGS reaction.

The quantification of the reducibility of the samples by comparing the experimentally consumed hydrogen to the theoretically needed one are presented in Table 2. For the theoretically needed H_2 calculations, as reducible components were considered Ce^{4+} and Cu^{2+} both reducing to Ce^{3+} and Cu°. For all samples incomplete reduction is observed. On the other hand taking into account the Raman observation for the possible Cu^{+} presence the reduction degree of the copper will be underestimated when calculated only on the basis of Cu^{2+}. The contrary is true for the Ce^{4+} which reduction is overestimated if the vacancy population associated to the Ce^{3+} increases. In any case, for the supported mixed oxides it is clear that with the increase of the Cu/Ce ratio the reducibility linearly decreases suggesting higher Cu/Ce interactions hindering the reduction process. The latter confirms the observations made on the cell contraction and solid solution formation by XRD.

In summary from the characterization data a number of interesting differences were identified between the $CuOCeO_2$ bulk catalyst and the alternative configuration using alumina as support for the mixed oxides. In terms of chemical composition the catalysts using alumina present much lower amount of active phase. The XRD data

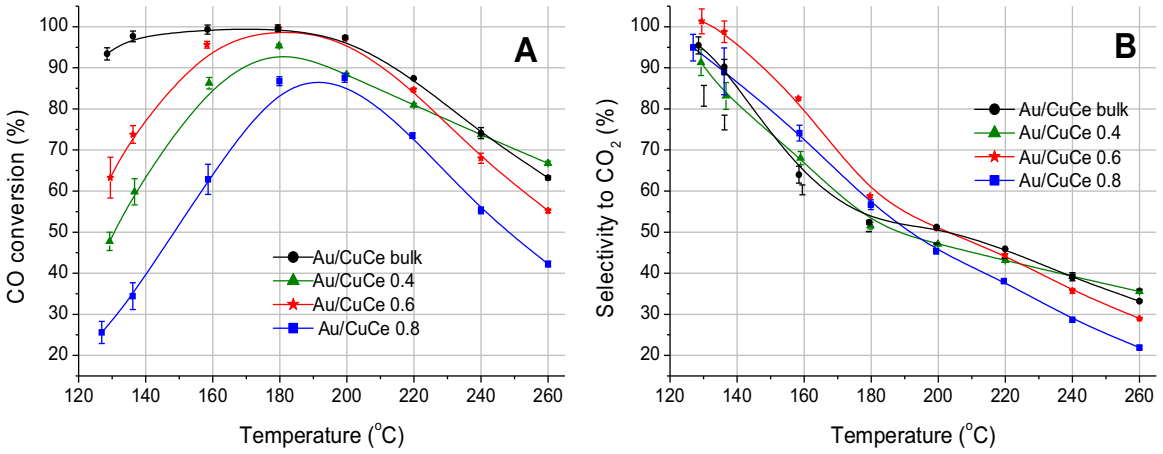

Fig. 8. Catalytic screening in the CO-PrOx reaction of the prepared gold promoted catalysts. (A) CO conversion; (B) selectivity towards CO_2.

reveal the formation of Cu-Ce solid solution for all the samples and a smaller ceria particle size for the samples supported in alumina. Very importantly, the oxygen vacancies population is boosted when copper-ceria are dispersed on the alumina as revealed by Raman. Furthermore, the samples promoted with gold shows a remarkable band gap contraction indicating a strong noble metal-support interaction and modified basicity. Finally, the systems dispersed on alumina seem to possess only surface reducibility while the CuCe bulk benefits both surface and bulk reducibility pointing to dissimilarities in terms of oxygen mobility among the bulk and alumina supported configurations.

3.6. WGS behaviour

Fig. 5A presents the catalytic screening in a model WGS mixture for the studied CuCe based catalysts. There are three very active samples in the shift process, namely CuCe-0.6, CuCe-0.8 and CuCe bulk while CuCe-0.4 shows medium-low activity. The main reason behind the poor activity of the CuCe-0.4 solid is the very low loading of active phases (around 10 wt.% CuO + CeO_2). Within the active samples, CuCe-0.8 is the most active sample exhibiting almost 90% of CO conversion from the very beginning of the reaction, an outstanding result for a WGS catalyst at low temperature. The excellent performance of this sample must be related to its superior concentration of oxygen vacancies as reflected on the O_v/F_{2g} ratio. As reported by Tabakova and co-workers there is a stretch correlation between oxygen vacancies and WGS activity [66]. It is a widespread opinion that water activation is the rate limiting step in the shift process [3,6]. In this sense, oxygen vacancies are viewed as the activation points to initiate the water splitting facilitating the reaction that afterwards proceed at the Cu/CeO_2 interface [19]. The CuCe bulk sample is also highly effective in the WGS validating its condition as reference material. However the fact that the CuCe-0.8 outperforms the activity displayed by the CuCe bulk sample demonstrates that advanced WGS catalysts with low active phase loading can be obtained when the copper-ceria mixed oxide is dispersed on a high surface carrier as Al_2O_3. This approach results advantageous form the economic and environmental point of view since high amounts of ceria and copper oxide are saved in the $CuOCeO_2/Al_2O_3$ configuration. Also it is worth noting that the activity of these "surface" dispersed mixed oxides increases linearly with Cu loading as shown in Fig. 5B. However the CuCe bulk with higher Cu loading is out of this trend underlining the superiority of the surface approach even with lower active phase content.

The activity of the gold promoted catalysts at the same conditions is depicted in Fig. 5C. The addition of gold affects differently the CuCe bulk compared to the alumina based catalysts. The activity of the CuCe bulk sample remarkably drops while the Al_2O_3 supported solid reflect an activity promotion. This result agrees with the chemical composition data presented in Table 1. CuCe bulk catalysts substantially losses CuO during gold deposition due to the highly basic media employed in the synthesis explicating the activity depletion. On the other hand, gold improves the CO conversion of the alumina based samples. Here it is worth noting that the most active sample CuCe-0.8 reaches the equilibrium conversion at 210 °C a better conversion value than that exhibited by a high performing Pt-ceria based catalysts measured at the same conditions [67]. Actually the gold promoted catalysts is an interesting multicomponent system with enhanced surface oxygen mobility and with a strong Au-CuO/CeO_2 interaction leading to favourable electronic properties which potentiate the WGS activity as elucidated from the TPR and UV–vis data.

When a fuel cell application is targeted the WGS reactor is usually placed downstream after the reforming unit. In this sense the presence of additional gases coming from the reforming process (mainly CO_2 and H_2) must be considered for a realistic WGS evaluation. Hence the catalytic screening in a realistic WGS mixture of the prepared Cu-Ce mixed samples is presented in Fig. 6A. Generally, all the curves are shifted towards higher temperatures as expected from the equilibrium restrictions and also for the competitive effect of CO_2 and H_2 hindering the access of CO and H_2O to the active sites. Again, as for the model WGS mixture CuCe-0.4 is the least active material while the rest of the catalysts exhibit a similar WGS behaviour. Apparently the CuCe-0.8 sample is the most active one in the low temperature range but it falls slightly behind the CuCe bulk catalysts from 300 °C onwards. In any case rather good CO conversions are obtained with the CuCe-0.8 and CuCe-0.6 especially considering their low copper and ceria loading.

The addition of gold (Fig. 6B) affects positively the alumina based catalysts and negatively to the CuCe bulk material for the same reasons commented above. Basically the $CuOCeO_2$ bulk is not as suitable as $CuOCeO_2/Al_2O_3$ for anchoring nanogold particles via DAE method since the noble metal deposition affects copper loading. Anyway, taking into account the demanding WGS mixture selected for this activity test, our catalysts can be considered rather effective for CO clean-up goals via WGS.

In order to obtain some semi-quantitative comparison of the samples during the reaction the specific reaction rates in the model WGS mixture were calculated, normalized on the active sites loading and expressed as $mol_{COconverted}/mol_{activesites}$ (Table 3). As active sites all the three components (Au, CuO and CeO_2) are considered due to the complex nature of the catalysts and the fact that every

component may play a role in the process [68]. These data provide a clearer idea of the different behaviour exhibited by the bulk system compared to the supported ones Although it should be considered that these data are an estimation of the apparent reaction rates aiming to normalize to some extension the catalytic activity. The specific activity of the supported materials is greater in all the cases (except for the CuCe-0,4). In other words, the mixed oxides dispersed on alumina seem to take better advantage of the active phases compared to the bulk one, an interesting result from the catalyst's optimization perspective. Moreover the presence of gold enhances the specific activity of the supported materials while affects negatively to the reaction rate presented by the bulk sample.

3.7. Preferential CO oxidation (CO-PrOx)

The equilibrium limitations of the WGS make necessary further CO removal to meet the PEM-FC operational requirements and CO-PrOx reaction results one of the most feasible alternatives in this regard. Our $CuOCeO_2$ catalysts were tested in a standard CO-PrOx mixture and the results in terms of activity and selectivity towards CO_2 are presented in Fig. 7A and B respectively. Very interestingly, the activity trends are rather different than those of the WGS reaction. In the low temperature window (130–200 °C) the CuCe bulk catalyst is clearly the best catalysts conserving practically full conversion at all the examined temperatures. Furthermore this catalyst at 130 °C displays an excellent activity/selectivity commitment with 98% of CO conversion and close to 95% of selectivity towards CO_2 formation. Nevertheless the CO conversion sequentially drops when the temperature surpasses 200 °C since at higher temperatures the rate of hydrogen oxidation exceeds that of carbon monoxide oxidation [69,70]

Curiously in the high temperature range, CuCe-0.4 becomes the most efficient sample showing elevated CO conversion and a completely different CO oxidation curve compared to those of the rest catalysts. In addition at 200 °C which is the only point in which CuCe-0.4 and CuCe bulk exhibit comparable conversions, the selectivity of the former is much higher than that of the later (76% *vs.* 52%) making the alumina based solid a better system for CO-PrOx at this conditions with a much lower amount of Cu and CeO_2 than the bulk $CuOCeO_2$ sample.

The addition of gold (Fig. 8) does not produce a great impact in the activity which confirms the superiority of $CuOCeO_2$ based catalysts over noble metals formulations for the CO-PrOx reactions in fair agreement with previous results in literature [21]. Only the CuCe-0.4 is positively influenced showing better activity in the low temperature range. For instance the CO conversion increases from 28% to 50% at 130 °C when gold was added. On the other hand, gold potentiates hydrogen combustion thus leading to poorer selectivity. Indeed this effect although it is not really marked on the studied samples can be observed by comparing the selectivity of CuCe-0.4 *vs.* Au/CuCe-0.4.

As for the WGS, CO-PrOx specific reaction rates were calculated and presented in Table 3. Very interestingly when the performance is discussed in terms of reaction rates the situation drastically changes and now the supported systems outperform the activity of the CuCe bulk. As shown in table CuCe-0.4 and Au/CuCe-0.4 present the highest specific activity. The obtained rates matches well with those of similar gold-ceria based catalysts recently reported [68]. This result reinforces the discussion derived from the WGS tests. The copper-ceria supported systems are intrinsically more active than the CuCe bulk. Although the overall CO conversion could be higher for the later the specific amount of CO converted by the former systems is always superior when the metallic loading are considered.

Finally if we try to merge the information derived from the WGS and CO-PrOx combined with the physicochemical properties of the studied materials, some relevant issues can be discussed. For example, being both reactions sensitive to the catalysts structure it seems that the WGS is more structure-dependent than the PrOx process. According to our findings, the best catalytic activity was achieved when the oxygen vacancies population was maximum and the ceria particle size minimum (CuCe-0.8 sample). This is due to key role of oxygen vacancies to carry out the water activation and also to the importance of the Cu–CeO_2 interface where most of the WGS reaction steps take place. In this regard, a smaller CeO_2 particle size involves a greater Cu–CeO_2 interface extension and more chances to develop the reaction. As a result when the structural properties of the catalysts are carefully adjusted, high performing WGS catalysts can be obtained with rather low active phase content. Apart from these chemical reasons some physical phenomena linked to alumina could contribute to the improved the WGS behaviour. For instance the enhanced textural properties provided by alumina may facilitate the transport and diffusion of water to the active sites of the catalyst.

On the other hand, CO-PrOx reaction is more sensitive to the $CuOCeO_2$ loading being the CuCe bulk the most active sample in terms of CO conversion. Actually is it hard to outperform the activity displayed by CuCe bulk at low temperature and this is the reason why this configuration is viewed as a benchmark catalyst for this reaction. Nonetheless, when the catalytic performance is normalized by the quantity of active phase involved in the process the supported systems are always superior to the reference CuCe for both WGS and CO-PrOx

4. Conclusions

Highly active catalysts for H_2 purification aims via WGS and CO-PrOx have been developed in this work. Our findings reveal that the $CuOCeO_2/Al_2O_3$ configuration can outperform the catalytic behaviour of the $CuOCeO_2$ bulk catalyst in the WGS reaction using much lower amount of active phase. The activity in the WGS is greatly influenced by the ceria oxygen vacancies population and the Cu/Ce ratio within the alumina based materials. In any case the catalysts designed in this work achieved elevated CO conversions in both model and realistic WGS mixtures.

For the PrOx reaction the bulk $CuOCeO_2$ catalyst performs better that the $CuOCeO_2/Al_2O_3$ in the low temperature range reaching almost full conversion and selectivity at 130 °C. However at temperatures above 200 °C some of the alumina based materials reached a better activity/selectivity balance opening new routes to explore in terms of global process efficiency.

The addition of gold promotes the reducibility of the $CuOCeO_2$ catalysts and generates and a strong noble metal-support interaction which tailors the electronic properties of the multicomponent systems. In general, gold benefits the alumina based materials at low temperatures in both reactions but results detrimental for the bulk configuration. Indeed, bulk $CuOCeO_2$ catalyst due to its high active phase loading barely needs the noble metal promotion.

Overall, in this paper the suitability of the $CuOCeO_2$ systems dispersed Al_2O_3 for both WGS and PrOx have been evidenced. The superiority of these materials is highlighted when the specific activities are calculated and referred to the total amount of active phase in the catalyst' formulation. Therefore, this approach results advantageous from the economic and environmental point of view since high amounts of mixed oxide are saved helping to extend the lifetime of ceria maybe for another 40 years of successful applications in catalysis.

Acknowledgements

Financial support for this work has been obtained from Junta de Andalucía (TEP-8196) and from the Spanish Ministerio de Economía y Competitividad (ENE2012-374301-C03-01 and ENE2013-47880-C3-2-R) co-financed by FEDER funds from the European Union.

References

[1] A.F. Ghenciu, Current Opin. Solid State Mater. 6 (2002) 389–399.
[2] A. Stephen, K. Hashmi, G.J. Hutchings, Angew. Chem. Int. Ed. 45 (2006) 7896–7936.
[3] J.A. Rodriguez, Catal. Today 160 (2011) 3–10.
[4] L. Barrio, A. Kubacka, G. Zhou, M. Estrella, A. Martínez-Arias, J.C. Hanson, M. Fernandez-Garcia, J.A. Rodriguez, J. Phys. Chem. C 114 (2010) 12689–12697.
[5] R. Jain, R. Maric, Appl. Catal. A Gen. 475 (2014) 461–468.
[6] C. Ratnasamy, J.P. Wagner, Catal. Rev. 51 (2009) 325–440.
[7] R.J. Farrauto, Y. Liu, W. Ruettinger, O. Ilinich, L. Shore, T. Giroux, Catal. Rev. 49 (2007) 141–196.
[8] E.T. Saw, U. Oemar, X.R. Tan, Y. Du, a. Borgna, K. Hidajat, S. Kawi, J. Catal, (2014) 32–46.
[9] G. Jacobs, S. Ricote, B.H. Davis, Appl. Catal. A Gen. 302 (2006) 14–21.
[10] P. Panagiotopoulou, D.I. Kondarides, Appl. Catal. B 101 (2011) 738–746.
[11] S. Colussi, L. Katta, F. Amoroso, R.J. Farrauto, A. Trovarelli, Catal Commun. 5 (2014) 63–66.
[12] F. Mariño, G. Baronetti, M. Laborde, N. Bion, A. Le Valant, F. Epron, D. Duprez, Int. J. Hydrogen Energy 33 (2008) 1345–1353.
[13] T. Tabakova, V. Idakiev, J. Papavasiliou, G. Avgouropoulos, T. Ioannides, Catal. Commun. 8 (2007) 101–106.
[14] Y. Li, Q. Fu, M. Flytzani-Stephanopoulos, Appl. Catal. B 27 (2000) 179–191.
[15] G. Avgouropoulos, T. Ioannides, H.K. Matralis, J. Batista, S. Hocevar, Catal. Lett. 73 (2001) 33–39.
[16] D.L. Trimm, Appl. Catal. A 296 (2005) 1–11.
[17] M. Boaro, M. Vicario, J. Llorca, C. Leitenburg, G. Dolcetti, A. Trovarelli, Appl. Catal. B 88 (2009) 272–282.
[18] I.D. González, R.M. Navarro, M.C. Álvarez-Galván, F. Rosa, J.L.G. Fierro, Catal. Commun. 9 (2008) 1759–1765.
[19] J.A. Rodriguez, J. Graciani, J. Evans, J.B. Park, F. Yang, D. Stacchiola, S. Senanayake, S. Ma, M. Pérez, P. Lui, J. Fdez Sanz, J. Hrbek, Angew. Chem. Int. Ed. 48 (2009) 8047–8050.
[20] J.A. Rodriguez, S. Ma, P. Liu, J. Hrbek, J. Evans, M. Pérez, Science 318 (2007) 1757–1760.
[21] G. Avgouropoulos, Ch. Ioannides Papadopoulou, J. Batista, S. Avgouropoulos, G. Hocevar, H.K. Matralis, Catal. Today 75 (2002) 157.
[22] G. Landi, P.S. Barbato, A. Di Benedetto, L. Lisi, Appl. Catal. B 181 (2016) 727–737.
[23] O.H. Laguna, M. González-Castaño, M.A. Centeno, J.A. Odriozola, Chem. Eng. J. 275 (2015) 45–52.
[24] G. Avgouropoulos, M. Manzoli, F. Boccuzzi, T. Tabakova, J. Papavasiliou, T. Ioannides, V. Idakiev, J. Catal. 256 (2008) 237–247.
[25] O.H. Laguna, W.Y. Hernández, G. Arzamendi, L.M. Gandía, M.A. Centeno, J.A. Odriozola, Fuel 118 (2014) 176–185.
[26] X. Liao, W. Chu, X. Dai, V. Pitchon, Appl. Catal. B 142–143 (2013) 25–37.
[27] T.R. Reina, S. Ivanova, M.A. Centeno, J.A. Odriozola, Int. J. Hydrogen Energy 40 (2015) 1782–1788.
[28] T.R. Reina, S. Ivanova, M.A. Centeno, J.A. Odriozola, Catal. Today 253 (2015) 149–154.
[29] S. Ivanova, C. Petit, V. Pitchon, Appl. Catal. A 267 (2004) 191–201.
[30] H. Li, L. Zhang, H. Dai, H. He, Inorg. Chem. 48 (2009) 4421–4434.
[31] P. Singh, M.S. Hegde, J. Solid State Chem. 181 (2008) 3248–3256.
[32] D.P. Volanti, D. Keyson, L.S. Cavalcante, A.Z. Simoes, M.R. Joya, E. Longo, J.A. Varela, P.S. Pizani, A.G. Souza, J. Alloy Compd. 459 (2008) 537–542.
[33] P. Djinovic, J. Batista, J. Levec, A. Pintar, Appl. Catal. A 364 (2009) 156–165.
[34] W. Liu, M. Flytzani-Stephanopoulos, J. Catal. 153 (1995) 317–332.
[35] K. Zhi, Q. Liu, R. Zhao, R. He, L. Zhang, J. Rare Earths 26 (2008) 538–543.
[36] R. Si, J. Raitano, N. Yi, L. Zhang, S.W. Chan, M. Flytzani-Stephanopoulos, Catal. Today 180 (2012) 68–80.
[37] F. Zhang, P. Wang, J. Koberstein, S. Khalid, S.-W. Chan, Surf. Sci. 563 (2004) 74–82.
[38] X.D. Zhou, W. Huebner, Appl. Phys. Lett. 79 (2001) 3512–3516.
[39] W. Liu, M. Flytzani-Stephanopoulos, J. Catal. 153 (1995) 304–316.
[40] B.M. Reddy, A. Khan, Y. Yamada, T. Kobayashi, S. Loridant, J.C. Volta, J. Phys. Chem. B 107 (2003) 11475–11484.
[41] E.O. Jardim, S. Rico-Francés, F. Coloma, J.A. Anderson, Enrique V. Ramos-Fernandez, J. Silvestre-Albero, A. Sepúlveda-Escribano, Appl. Catal. A 492 (2015) 201–211.
[42] G.W. Graham, W.H. Weber, C.R. Peters, R. Usmen, J. Catal. 130 (1991) 310–313.
[43] J.Z. Shyu, W.H. Weber, H. Gandhi, J. Phys. Chem. 92 (1988) 4964–4970.
[44] J.R. McBride, K.C. Hass, B.D. Poindexter, W.H. Weber, J. Appl. Phys. 76 (1994) 2435–2441.
[45] P.Y. Yu, Y.R. Shen, Y. Petroff, Solid State Comm. 12 (1973) 973–975.
[46] P.F. Williams, S.P. Porto, Phys. Rev. 8 (1973) 1782–1785.
[47] X.M. Lin, L.P. Li, G.S. Li, W.H. Su, Mater. Chem. Phys. 69 (2001) 236–240.
[48] J.E. Spanier, R.D. Robinson, F. Zheng, S.W. Chan, I.P. Herman, Phys. Rev. B 64 (2001) 245407 (245401–245408).
[49] W.Y. Hernandez, M.A. Centeno, F. Romero-Sarria, J.A. Odriozola, J. Phys. Chem. C 113 (2009) 5629–5635.
[50] J.F. Xu, W. Ji, Z.X. Shen, S.H. Tang, J. Solid State Chem. 147 (1999) 516–519.
[51] W. Wang, Q. Zhou, X. Fei, Y. He, P. Zhang, G. Zhang, L. Peng, W. Xie, Cryst. Eng. Commun. 12 (2010) 2232–2237.
[52] O.H. Laguna, F. Romero-Sarria, M.A. Centeno, J.A. Odriozola, J. Catal. 276 (2010) 360–370.
[53] V. Petrovsky, B.P. Gorman, H.U. Anderson, T. Petrovsky, J. Appl. Phys. 90 (2001) 2517–2521.
[54] G.W. Li, L. Hong, M.S. Tong, H.H. Deng, X.-H. Xia, W. Chen, Anal. Methods 7 (2015) 1924–1928.
[55] A. Bensalem, J.C. Muller, F. Bozon-Verdura, J. Chem. Soc. Faraday Trans. 88 (1) (1992) 153–154.
[56] M.H. Groothaert, J.A. van Bokhoven, A. Battiston, B.M. Weckhuysen, R.J. Schoonheydt, J. Am. Chem. Soc. 125 (2003) 7629–7640.
[57] N. Pestryakov, N. Bogdanchikova, A. Simakov, I. Tuzovskaya, F. Jentoft, M. Farias, A. Díaz, Surf. Sci. 601 (2007) 3792–3795.
[58] El-Sayed Mostafa, J. Appl. Sci. 5–10 (2005) 1867–1870.
[59] N. Imanaka, T. Masui, H. Hirai, G.-Y. Adach, Chem. Mater. 15 (2003) 2289–2291.
[60] C.T. Campbell, Nature Chem. 4 (2012) 597–598.
[61] A. Bruix, J.A. Rodriguez, P.J. Ramírez, S.D. Senanayake, J. Evans, J.B. Park, D. Stacchiola, P. Liu, J. Hrbek, F. Illas, J. Am. Chem. Soc. 134 (2012) 8968–8974.
[62] L. Pastor-Pérez, R. Buitrago-Sierra, A. Sepúlveda-Escribano, Int. J. Hydrogen Energy 39 (2014) 17589–17599.
[63] Q. Fu, S. Kudriavtseva, H. Saltsburg, M. Flytzani-Stephanopoulos, Chem. Eng. J. 93 (2003) 41–53.
[64] D. Andreeva, I. Ivanov, L. Ilieva, J.W. Sobczak, G. Avdeev, T. Tabakova, Appl. Catal. A 333 (2007) 153–160.
[65] G. Jacobs, E. Chenu, P.M. Patterson, L. Williams, D. Sparks, G. Thomas, B.H. Davis, Appl. Catal. A 258 (2004) 203–214.
[66] T. Tabakova, M. Manzoli, D. Paneva, F. Boccuzzi, V. Idakiev, I. Mitov, Appl. Catal. B 101 (2011) 266–274.
[67] M. Gonzalez Castaño, T.R. Reina, S. Ivanova, M. a. Centeno, J.A. Odriozola, J. Catal. 314 (2014) 1–9.
[68] T.R. Reina, C. Megias-Sayago, A. Perez, S. Ivanova, M.A. Centeno, J.A. Odriozola, J. Catal. 326 (2015) 161–171.
[69] A. Luengnaruemitchai, S. Osuwan, E. Gulari, Int. J. Hydrogen Energy 29 (2004) 429–435.
[70] D.H. Lee, D.H. Kim, Catal. Today 132 (2008) 109–116.